JOURNAL OF CATALYSIS **171,** 130–147 (1997)
ARTICLE NO. CA971777

Isobutanol and Methanol Synthesis on Copper Catalysts Supported on Modified Magnesium Oxide

Mingting Xu, Marcelo J. L. Gines, Anne-Mette Hilmen, Brandy L. Stephens, and Enrique Iglesia[1]

Department of Chemical Engineering, University of California at Berkeley, Berkeley, California 94710

Received January 27, 1997; revised June 9, 1997; accepted June 10, 1997

Alcohols are selectively produced from CO/H_2 on $K-CuMgCeO_x$ catalysts, but synthesis rates are strongly inhibited by CO_2 formed during reaction. Reaction pathways involve methanol synthesis on Cu, chain growth to C_{2+} alcohols, and metal–base bifunctional coupling of alcohols to form isobutanol. Ethanol reactions on $K-Cu_{0.5}Mg_5CeO_x$ show that Cu catalyzes both alcohol dehydrogenation and aldol condensation reactions. CeO_2 increases Cu dispersion and MgO surface area and K decreases Cu dispersion, but increases the density of basic sites. Reactions of acetaldehyde and ^{13}C-labeled methanol lead to 1-^{13}C-propionaldehyde, a precursor to isobutanol. The density and strength of basic sites were measured using a $^{12}CO_2/^{13}CO_2$ isotopic jump method that probes the number and chemical properties of basic sites available at typical isobutanol synthesis temperatures. K or CeO_2 addition to $CuMgO_x$ increases the density and strength of basic sites and the rates of base-catalyzed ethanol condensation reactions leading to acetone and *n*-butyraldehyde. The presence of CO in the He carrier during temperature-programmed surface reactions of ethanol preadsorbed on $Cu_{0.5}Mg_5CeO_x$ decreases the rate of base-catalyzed condensation reactions of preadsorbed ethanol, possibly due to the poisoning of basic and Cu sites by the CO_2 formed from CO via water–gas shift reactions.

INTRODUCTION

Isobutanol is a potential fuel additive and a precursor to isobutene and methyl-*tert*-butyl ether. Currently available catalysts for the synthesis of isobutanol from CO/H_2 mixtures require high temperatures (750–800 K) and pressures (10–30 MPa) and produce isobutanol with relatively low productivity and selectivity under milder reaction conditions (1–5). Typical isobutanol yields reported in the literature are shown in Table 1.

Isobutanol synthesis requires the initial formation of methanol and higher linear alcohols and their subsequent chain growth processes leading to 2-methyl-branched alcohols with high selectivity (3). Chain growth rates are low for 2-methyl-1-propanol (isobutanol) because of its steric hindrance and the lack of the two α-hydrogens required for aldol condensation reactions. Therefore, isobutanol becomes a preferred end product of alcohol chain growth reactions on basic oxides. Isobutanol synthesis appears to be limited by the rate of ethanol formation from synthesis gas (4, 6), which limits the concentration of the aldehydic intermediates required for chain growth. High reactor pressures favor the synthesis of higher alcohols and bimolecular condensation reactions during CO hydrogenation, but lead to unfavorable thermodynamics for alcohol dehydrogenation steps that may be required in order to form aldehyde intermediates required in aldol coupling pathways.

Our study addresses the reaction pathways and catalytic site requirements for the synthesis of branched alcohols on (metal–base) bifunctional catalysts at low temperatures. These bifunctional catalysts consist of Cu metal crystallites supported on high-surface-area basic oxides based on modified MgO. Specifically, we describe the synthesis procedures, catalyst structural characterization data, and surface and catalytic properties for a class of materials based on K-modified $CuMgCeO_x$ (6–8). These $K-CuMgCeO_x$ catalysts are among the best reported catalysts for alcohol synthesis at low temperatures and pressures (6–8). MgO-based solids also catalyze condensation reactions of alcohols and aldehydes with high activity and selectivity (9, 10).

$CuMgCeO_x$ samples were prepared by controlled pH coprecipitation methods designed to maximize the number of Cu surface atoms and basic sites (8). Site titration and isotopic switch methods were used to determine the density and chemical properties of exposed Cu and basic sites. Isobutanol and linear alcohol synthesis pathways were studied using the adsorption and surface reactions of alcohols and aldehydes in steady-state catalytic reactors and in a temperature-programmed surface reaction (TPSR) apparatus. The role of individual elements in multicomponent catalysts was explored by varying the composition of $K-CuMgCeO_x$ catalysts and determining the effect of each component on surface properties and on reaction steps.

[1] To whom correspondence should be addressed. E-mail: iglesia@cchem.berkeley.edu. Fax: (510) 642-4778.

0021-9517/97 $25.00

TABLE 1

Representative Isobutanol Synthesis Catalysts (6, 7)

Catalyst	T (K)	P (MPa)	CO/H_2	GHSV (h^{-1})	Isobutanol yield ($g/kg_{cat}/h$)
Cu–Zn–Cr–Cs	583	9.1	1.0/0.45	5330	51
Cu–Mg–Ce–K	593	5.1	1.0/1.0	1832	7.2
Pd–Zr–Zn–Mn–Li	593	5.1	1.0/1.0	1832	1.1
Cu–Zn–Mn–K	643	10.0	0.5/1.0	10000	175[a]
Zn–Cr–K	693	32.5	1.0/2.2	15000	125[a]
Pd–Zr–Zn–Mn–Li	700	25.0	1.0/1.0	20000	740[a]

[a] $g/liter_{cat}/h$.

EXPERIMENTAL METHODS

Catalyst Synthesis

$CuMgCeO_x$ samples were prepared by coprecipitation of mixed nitrate solutions with an aqueous solution of KOH (2 *M*) and K_2CO_3 (1 *M*) at 338 K and a constant pH of 9 in a well-stirred thermostated container. The solids formed were filtered, washed thoroughly with 300–500 cm^3 of deionized water at 333 K, and dried at 353 K overnight. Dried samples were treated in flowing air at 723 K for 4 h in order to form the corresponding mixed metal oxides. Residual potassium in all dry samples was less than 0.1 wt.% before alkali impregnation. The controlled pH coprecipitation technique produces uniform precipitates, which lead, after thermal treatment, to mixed metal oxides with high surface area and intimate contact between components (8). $CuZnAlO_x$ samples were prepared using the same procedures as for $CuMgCeO_x$, except that the pH was held at 7.0 and the dried powders were treated in flowing air at 623 K for 4 h (11, 12). K and Cs were introduced by incipient wetness of the oxidized samples using K_2CO_3 (0.25 *M*) and CH_3COOCs (0.25 *M*) aqueous solutions (K_2CO_3: Fisher Scientific, A.C.S. certified; CH_3COOCs: Strem Chemicals, 99.9%).

Structural Characterization

Powder X-ray diffraction (XRD) patterns were collected using a D5000 Siemens Diffractometer and monochromatic Cu-$K\alpha$ radiation. Total surface areas were determined using the single point BET method by measuring N_2 physisorption at 77 K using a continuous flow Quantasorb Surface Area Analyzer (Quantachrome Corp.). Bulk catalyst compositions were measured by atomic absorption spectroscopy (AAS).

The reduction behavior of Cu catalysts was studied using temperature-programmed reduction (TPR). This method involves treating a Cu sample (15–100 mg) in He at 723 K for 0.3 h in order to remove adsorbed water and carbonates. Different amounts of samples were used for the high- and low-Cu catalysts in order to get the same amount of CuO charge in the reactor. After the temperature was lowered to 300 K, a 5% H_2/He mixture (100 cm^3/min) was introduced into the reactor and the temperature was then increased to 623 K at a rate of 0.17 K/s. The evolution of H_2O and the consumption of H_2 during reduction were followed by on-line mass spectrometry (H200M Gas Analyzer, Leybold Inficon Inc.).

Site Density and Reactivity

Cu surface areas were measured by titrating Cu surface atoms in prereduced samples with N_2O (Matheson, ultra high purity) at 363 K. N_2O was introduced as pulses (1.60 μmol N_2O/pulse) into a He stream. The number of chemisorbed O atoms was obtained from the amount of N_2O consumed and the N_2 produced. A saturation coverage of 0.5 : 1 O : Cu_s was used to estimate Cu surface area and dispersion (13, 14). Cu dispersion is defined as the ratio of surface Cu (Cu_s) to the total number of Cu atoms in the catalyst.

In temperature-programmed CO_2 desorption (TPD) measurements, samples (50 mg) were first pretreated in flowing He ($\sim$100 cm^3/min) at 723 K for 0.3 h and then reduced in 5% H_2/He at 623 K for 0.5 h. After exposure to CO_2 (Cambridge Isotope Laboratories, Inc.) for 0.15 h at room temperature, the samples were flushed with He to remove gas phase and weakly adsorbed CO_2. The temperature was then increased up to 723 K at a rate of 0.5 K/s, and the desorption profile of CO_2 was monitored by mass spectrometry.

The density of basic sites was determined using a $^{13}CO_2/^{12}CO_2$ isotopic exchange method. This method provides a direct measure of the number of basic sites kinetically available for CO_2 adsorption at typical reaction temperatures. This technique also provides the reactivity distribution of basic sites and a direct measure of surface nonuniformity. In this method, a prereduced catalyst was exposed to a 0.1% $^{13}CO_2$/0.1% Ar/He (Cambridge Isotope Laboratories, Inc.) stream at 573 K. After $^{13}CO_2$ reached a constant concentration in the effluent stream (0.5 h), the flow was switched to 0.1% $^{12}CO_2$/He (Cambridge Isotope Laboratories, Inc.). The decay in the concentration of $^{13}CO_2$ as it was replaced on the surface by $^{12}CO_2$ was followed by mass spectrometric analysis of $^{13}CO_2$ and Ar concentrations as a function of the time elapsed after the isotopic switch. The presence of Ar permitted corrections for gas holdup and hydrodynamic delays within the apparatus.

Temperature programmed surface reaction studies were carried out by exposing a prereduced catalyst (33.0 mg) to an ethanol/He stream at room temperature for 0.2 h. Ethanol (C_2H_5OH: Fisher Scientific, A.C.S. certified) was introduced by passing He through a saturator containing ethanol at 273 K. The catalyst sample was then purged with

He (100 cm^3/min) at room temperature in order to remove gas phase and weakly adsorbed species and the reactor temperature was increased to 723 K at 0.5 K/s. Desorption products were continuously monitored by mass spectrometric analysis of the effluent stream. The TPSR apparatus and the detailed experimental procedures will be described elsewhere (15). H_2 and He were purified by passing through a molecular sieve trap (Matheson, Model 452 : 4A) in order to remove H_2O and through an oxygen scavenging trap (Matheson, Model 64-1008A).

Catalytic Evaluation and Mechanistic Studies

High-pressure isobutanol synthesis studies were performed in a catalytic microreactor consisting of a single-pass tubular reactor (1.27 × 0.071 cm, 304 stainless-steel tube, length 33.0 cm) held within a three-zone heated furnace in order to ensure uniform axial temperatures (±1 K). The catalyst (2 g) was reduced *in situ* in pure H_2 (Matheson, 99.99%) at 583 K and atmospheric pressure for 12 h before catalytic experiments were carried out at 4.5 MPa using synthesis gas (H_2/CO/Ar = 0.45/0.45/0.10 at.; Matheson: 99.99% CO, 99.99% Ar). Ar was used as an internal standard in order to ensure accurate material balances. Synthesis gas was purified using activated carbon (Sorb-Tech RL-13) in order to remove metal carbonyls. H_2 was purified by passing through a catalytic purifier (Matheson, Model 64-1008). Traces of water were removed from H_2 and H_2/CO mixtures using molecular sieves (Matheson, Model 452 : 4A).

Reactants and products were analyzed on-line using a gas chromatograph (Hewlett–Packard, Model 5890 II Plus) equipped with a 10-port sampling valve and two sample loops. One sample loop was injected into a 5% phenyl-methyl-silicone capillary column (HP-5, 50 m, 0.32 mm diameter, 1.05 μm film thickness) and the other into a packed column (Porapak Q, 1.8 m length, 0.32 cm diameter). A thermal conductivity detector (TCD) was used to measure the concentration of Ar, N_2, CO, CO_2, and H_2O in the effluent from the packed column. A flame ionization detector (FID) was used to measure the concentrations of all organic compounds eluting from the capillary column. Condensable products were collected and used to confirm the identity of species in reaction products by mass spectroscopic analysis after capillary chromatography (Hewlett–Packard, Model 5890 II Plus GC; Hewlett–Packard, Model 5972 Mass Selective Detector).

Alcohol and aldehyde coupling reactions were carried out in a gradientless recirculating reactor unit (RRU). The catalyst (18.0 mg) was first reduced in H_2 (10% H_2/He) at 623 K for 0.5 h. The temperature was lowered to 573 K and ethanol was introduced along with a small amount of methane, used as an unreactive internal standard (reaction mixture: $C_2H_5OH/CH_4/He$ = 4.0/2.7/94.6 kPa; C_2H_5OH: Fisher Scientific, A.C.S. certified; CH_4: Matheson, ultra high purity). The reactant mixture was circulated continuously through the catalyst sample and reaction products were sampled by syringe extraction after various contact times. Reactant and product concentrations were measured by mass spectrometric and flame ionization detection, after separation with a 5% phenyl-methyl-silicone capillary column. The effect of CO_2 (Matheson: research grade) during ethanol reactions on 1 wt.% K–$Cu_yMg_5CeO_x$ was explored by adding different amounts of CO_2 (0–20 kPa) to the ethanol reactants. Cross-coupling reactions of $^{13}CH_3OH$ (^{13}C: 99%, ^{18}O: 12%; Isotec Inc.) with acetaldehyde (Fisher Scientific, Reagent Grade) were carried out using the following reactant mixture: $^{12}C_2H_4O/^{13}CH_3OH/CH_4/He$ = 4.0/8.0/2.7/86.6 kPa. $^{13}CH_3OH$ was purified by several freeze–pump–thaw cycles before catalytic experiments.

RESULTS AND DISCUSSION

Structural and Textural Properties of K–CuMgCeO$_x$ Catalysts

The X-ray diffraction pattern of a dried precipitate sample shows the presence of $Mg(OH)_2$ and $Ce(OH)_4/CeO_2$ phases (Fig. 1a). The poor sample crystallinity and the coincidence of diffraction lines for Ce oxide and hydroxide phases make it difficult to determine conclusively the form of Ce in dried samples. Precipitates did not show any diffraction lines corresponding to layered hydrotalcite-type structures.

Separate MgO and CeO_2 phases were detected by X-ray diffraction after air treatment at 723 K (Fig. 1b). Diffraction lines occurred at the positions expected for the pure monometallic oxides and provided no evidence for $MgCeO_x$ mixed oxides. CuO crystallites were not detected, suggesting that the Cu component is well dispersed, either

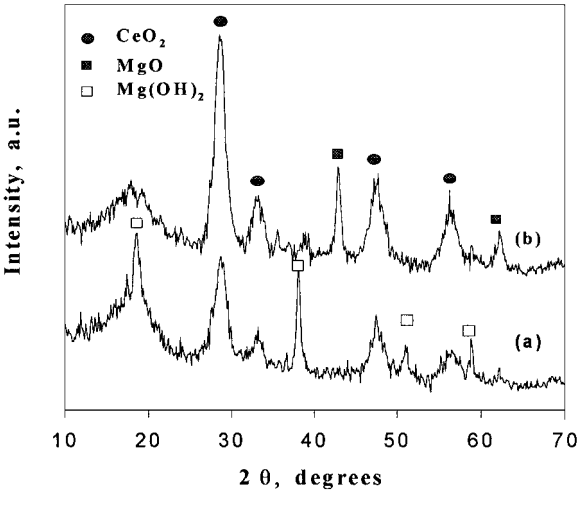

FIG. 1. Powder X-ray diffraction patterns of Cu/Mg/Ce = 0.5/5.0/1.0 (atomic ratio) samples (a) uncalcined and (b) treated in air at 723 K.

TABLE 2

Composition, Surface Area, and Basic Site Density of Mixed Metal Oxides

Sample	K content[a] (wt.%)	BET surface area (m^2/g)	Cu dispersion[b]	Exchangeable CO_2 at 573 K (10^{-6} mol/m^2)	CO_2 desorbed during TPD below 573 K (10^{-6} mol/m^2)	CO_2 exchange rate constant[c] (k, $\times 10^3$ s^{-1})
MgO	0.01	191	—	0.38	0.50	18
$Cu_{0.1}MgO_x$	0.2	118	0.06	—	—	—
Mg_5CeO_x	0.01	188	—	0.95	0.84	5.0
$Cu_{0.5}Mg_5CeO_x$	0.1	167	0.23	1.2	0.62	4.8
$Cu_{0.5}Mg_5CeO_x$	1.0	147	0.14	2.3	0.64	2.4
$Cu_{0.5}Mg_5CeO_x$	3.5	62	0.062	5.2	0.65	2.6
$Cu_{7.5}Mg_5CeO_x$	1.2	92	0.047	3.3	0.91	3.0
$Cu/ZnO/Al_2O_3$	0	62	0.05	1.1	0.72	13

[a] Bulk composition measured by atomic absorption.

[b] Dispersion calculated from the ratio of surface Cu (determined by N_2O decomposition at 363 K (13, 14)) to the total number of Cu atoms in the catalyst.

[c] Obtained at the peak maximum of basic site distribution curve.

as small crystallites or as a solid solution within the CeO_2 lattice. Mixed Cu/Ce oxide solid solution can form during coprecipitation and remain after high temperature oxidative treatments (16, 17).

The total surface area of $Cu_{0.5}Mg_5CeO_x$ samples decreased with increasing K concentration (Table 2). Lunsford and co-workers (18, 19) have reported that the addition of Li also decreases the surface area of MgO. The copper dispersion measured by N_2O decomposition on $Cu_{0.5}Mg_5CeO_x$ is 0.23 (Table 2); this value is among the highest reported in the literature for Cu-based methanol and higher alcohol synthesis catalysts. This copper dispersion value corresponds to a crystallite size of about 5 nm assuming hemispherical crystals. A $Cu_{0.5}Mg_5O_x$ sample with similar Cu content as $Cu_{0.5}Mg_5CeO_x$ has a copper dispersion of only 0.06. Thus, the presence of Ce oxide species favors the formation of small Cu metal crystallites on MgO supports.

The decomposition of N_2O on reduced ZnO sites has been found to corrupt Cu surface area measurements on Cu/ZnO catalysts (20). It is possible that decomposition of N_2O on reduced CeO_x species in prereduced $Cu_{0.5}Mg_5CeO_x$ catalysts also corrupts N_2O titration data and leads to observed high copper dispersion values. N_2O did not decompose on Mg_5CeO_x samples prereduced at 623 K, suggesting that any reduced Ce species present do not decompose N_2O at 363 K. CeO_2 may only reduce, however, when Cu metal is available in order to dissociate H_2. In effect, the presence of Cu may promote the reduction of CeO_2.

A reduction–oxidation cycle was carried out in order to rule out any contribution from reduced Ce species to N_2O titration measurements of Cu surface area. A $Cu_{0.5}Mg_5CeO_x$ sample was reduced at 623 K and N_2O titration data were obtained. The measured Cu surface area was found to be 19.0 m^2/g (0.23 Cu dispersion). This sample was rereduced at 473 K instead of 623 K after the titration measurements. Surface oxygen atoms on Cu surface can be removed at 473 K in H_2, but reduction of CeO_2 is likely to occur only at higher reduction temperatures. Thus, reduction at 473 K should remove oxygen from Cu surface but not from CeO_x. The Cu surface area of the sample reduced at 473 K was 19.3 m^2/g, a value identical to that obtained on the fresh sample after reduction at 623 K (19.0 m^2/g). This shows that CeO_x does not contribute to the measured copper dispersion and that measured dispersion values indeed reflect the presence of very small Cu metal crystallites of diameter about 5 nm. An additional exposure of this titrated sample to 5% H_2 at 423 K resulted in a Cu surface area of 17.9 m^2/g, suggesting that oxygen atoms chemisorbed on Cu can be almost completely removed by H_2 at temperatures as low as 423 K.

Copper dispersion decreased with increasing K loading (Table 2) because of a decrease in the surface area of the Mg_5CeO_x support and also because K species may block surface Cu atoms or inhibit their reduction to Cu metal, resulting in a decrease in the number of exposed surface Cu atoms. CeO_x addition to $Cu_{0.1}MgO_x$ increased both surface area and copper dispersion (Table 2), suggesting that CeO_x acts as structural promoter.

The temperature-programmed reduction profiles of MgO-based Cu samples are shown in Fig. 2. The onset and peak maximum temperatures for H_2 consumption and H_2O formation appeared at the same temperature for each sample. The high-temperature tail in the H_2O peak is caused by a strong interaction between H_2O and MgO. This tail was not observed for the H_2 peak, but the signal-to-noise ratio of the H_2 peak was lower than that of H_2O because of the high H_2 background pressure in the mass spectrometer.

The presence of CeO_x in $Cu_{0.5}Mg_5CeO_x$ decreases the reduction temperature of CuO (from 508 to 436 K). CeO_x addition also increases Cu dispersion and decreases Cu

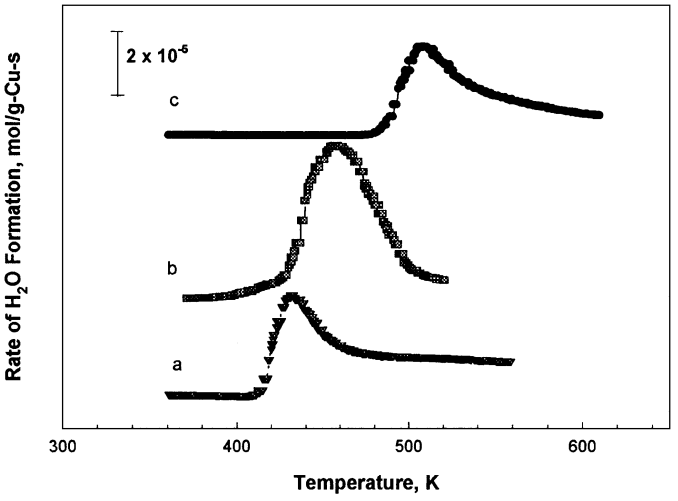

FIG. 2. Temperature-programmed reduction profiles obtained in 5% H_2/He of MgO-based Cu catalysts: (a) $Cu_{0.5}Mg_5CeO_x$; (b) $Cu_{7.5}Mg_5CeO_x$; (c) $Cu_{0.1}Mg_5O_x$. [Heating rate: 0.17 K/s; 15–100 mg of sample, 100 cm^3/min 5% H_2/He mixture; pretreatment temperature, 723 K.]

particle size apparently because of strong interactions between Cu and CeO_x. The large Cu particles in $Cu_{7.5}Mg_5CeO_x$, however, can also be reduced at temperature lower than that on $Cu_{0.1}MgO_x$. The reduction profiles (Fig. 2) suggest that the promoting effect of CeO_x on copper oxide reduction increases with increasing Ce/Cu ratio. CeO_x has been reported previously to promote metal oxide reduction for $Pd/CeO_2/Al_2O_3$ catalysts (21). The presence of CeO_x shifts the reduction peak temperature of PdO from 437 to 376 K. Moreover, the reduction behavior of a $Pd/CeO_2/Al_2O_3$ sample prepared by the coprecipitation of Pd and cerium nitrates differs from that of a $Pd/CeO_2/Al_2O_3$ prepared by successive impregnation of Al_2O_3 with CeO_2 and Pd. Some reduction occurs at room temperature on the sample prepared by the coprecipitation methods as a consequence of a higher degree of PdO–CeO_x contact area (22). Lamonier *et al.* (16) have found that Cu^{2+} insertion into CeO_x occurs during the synthesis of $CuCeO_x$ samples by coprecipitation methods. Four different species, present as CuO monomers, dimers, clusters, and small particles, were detected in these CuO/CeO_2 samples (16).

ZnO has a similar effect as CeO_x on copper reduction. Garcia-Fierro *et al.* (22, 23) reported that the fraction of copper oxide strongly interacting with ZnO increases with increasing Zn/Cu ratio and that such copper oxide species reduced a low temperature. A kinetic model of reduction kinetics of CuO/ZnO suggests that the promoting effect of ZnO on copper reduction is caused by the dissociative adsorption of H_2 on ZnO surfaces or on Cu metal clusters closely associated with ZnO (24). The spillover of the hydrogen atoms formed enhances Cu^{2+} reduction. In fact, kinetic analysis showed that the apparent activation energy, E_a, was 84 kJ/mol for the reduction of pure CuO whereas E_a decreased to 77 kJ/mol for the reduction of the CuO–ZnO catalysts (22), in agreement with the promoting effect of ZnO on the reducibility of CuO. Similar processes are likely to occur during CuO reduction on $CuMgCeO_x$ samples. A better contact between CeO_x and Cu is expected with increasing CeO_x/Cu ratio, leading to CuO reduction at lower temperatures.

In contrast with CeO_x , K addition to Cu-containing samples inhibits CuO reduction, as shown by the shift of the reduction peak to higher temperatures (Fig. 3). The effect of K is stronger on low-Cu ($Cu_{0.5}Mg_5CeO_x$; $\Delta T = 79$ K) than on high-Cu ($Cu_{7.5}Mg_5CeO_x$; $\Delta T = 57$ K) catalysts. Also, the effect of K did not depend on the presence of CeO_x; the reduction temperatures increased to a similar extent ($\Delta T =$ 70 K) on K–$Cu_{0.5}Mg_5O_x$ and K–$Cu_{0.5}Mg_5CeO_x$. K appears to increase the stability of Cu^{2+} ions and to make them more difficult to reduce by H_2. A similar effect was reported on Cs-promoted $Cu/ZnO/Cr_2O_3$ (25). In this study, the presence of Cs retards CuO reduction by about 50 K. Campos-Martin *et al.* (25) suggest that the inhibited reduction of CuO is associated to closer interaction between the CuO and alkali phases retards H_2 activation.

The observed inhibition of copper reduction by K can be explained by inhibited activation of H_2, as proposed by Klier and co-workers (25), or by the strengthening of Cu–O bonds upon K addition. As reported in the literature (26, 27), the bond energy of surface oxygen for CuO is about 42 kJ/mol and it increases to 63 kJ/mol upon the addition of 10–25 at.% MgO. Addition of MgO weakens the Cu–Cu bonds and strengthens Cu–O bonds. In a similar way, the incorporation of K_2O into CuO during catalyst synthesis may

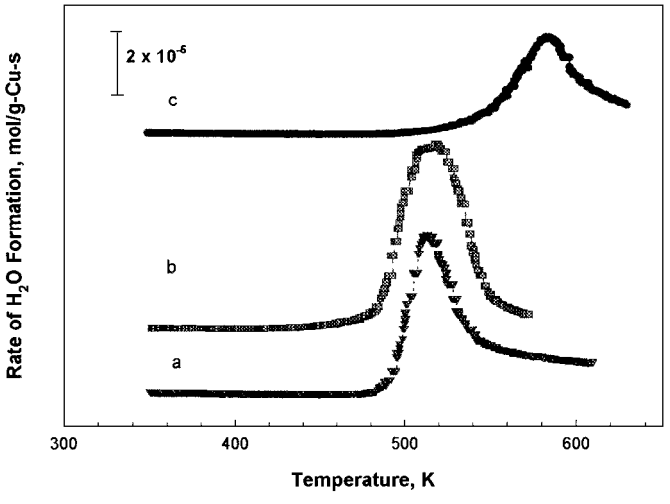

FIG. 3. Temperature-programmed reduction profiles obtained in 5% H_2/He of MgO-based Cu catalysts: (a) 1.0 wt.% K–$Cu_{0.5}Mg_5CeO_x$; (b) 1.2 wt.% K–$Cu_{7.5}Mg_5CeO_x$; (c) 1.1 wt.% K–$Cu_{0.1}Mg_5O_x$. [Heating rate: 0.17 K/s; 15–100 mg of sample, 100 cm^3/min 5% H_2/He mixture; pretreatment temperature, 723 K.]

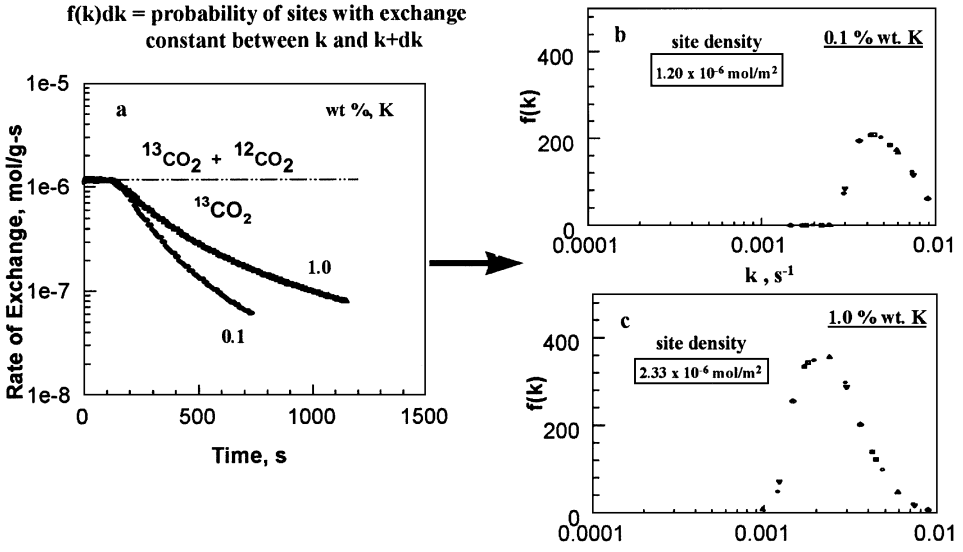

FIG. 4. Isotopic switch method for probing adsorption–desorption processes dynamics on nonuniform surface of K–$Cu_{0.5}Mg_5CeO_x$.

increase the bond strength of Cu–O and therefore retard CuO reduction.

Density and Strength of Basic Sites

The density and strength of basic sites on modified MgO samples were measured from the exchange capacity and rates obtained using isotopic $^{13}CO_2/^{12}CO_2$ switch experiments at typical reaction temperatures (573 K). Site densities obtained from the area under the $^{13}CO_2$ relaxation curves are shown in Table 2 for several catalytic materials. As a comparison, basic site densities determined by TPD of preadsorbed CO_2 are also listed in Table 2. CO_2 TPD measurements involve the adsorption of CO_2 on prereduced samples at room temperature, the removal of gas phase and weakly adsorbed CO_2 by flowing He, and a linear temperature increase with on-line monitoring of the CO_2 evolution rate by mass spectrometry. CO_2 TPD basic site densities were obtained by integration of the evolution rate curves up to a desorption temperature of 573 K.

Although temperature-programmed desorption of CO_2 is frequently used for measuring basic site densities and strength, the area under TPD curves gives the total number of basic sites and not the number of basic sites kinetically available for adsorption and catalytic reaction at reaction temperature. Desorption peak temperatures provides only qualitative information about the basic strength. In contrast, $^{13}CO_2/^{12}CO_2$ exchange methods can provide not only a direct measure of the number of these basic sites that reversible chemisorb CO_2 at 573 K, but also a distribution of reactivity for such basic sites (28).

The relaxation responses obtained from $^{13}CO_2/^{12}CO_2$ isotopic switch experiments on $Cu_{0.5}Mg_5CeO_x$ catalysts with 0.1 and 1.0 wt.% K are shown in the semi-logarithmic plots of Fig. 4a. The exchange capacity is determined from the area of the $^{13}CO_2$ desorption curve immediately after a switch from $^{13}CO_2$ to $^{12}CO_2$. When corrected for gas holdup, physical hydrodynamic delays, and CO_2 mass spectrometric response factors, this area corresponds to the number of basic sites that are kinetically accessible for exchange reactions at 573 K. Weakly interacting sites are mostly unoccupied by CO_2; strongly interacting sites do not exchange in the time scale of the isotopic relaxation experiment. These strongly interacting and weakly interacting sites are also unlikely to contribute to catalytic reactions at 573 K. Site densities obtained from these measurements are shown in Table 2.

The local slope in the semi-logarithmic plots of Fig. 4a reflects the dynamics of the first-order CO_2 exchange reaction and thus the exchange rate constant on available basic sites. The curved semi-logarithmic plots show that $Cu_{0.5}Mg_5CeO_x$ surfaces contain sites with a distribution of exchange rate constants, because uniform surfaces with only one type of adsorption site would lead to straight lines in Fig. 4a. Exchange rate constants depend on the thermodynamics of binding interactions between CO_2 and basic sites through linear free energy relations commonly used to estimate activation energies for chemical reactions (29). Large exchange rate constants and the concomitant short relaxation times (e.g. on 0.1 wt.% K) reflect short CO_2 surface lifetimes and weaker binding of CO_2 molecules on available basic sites.

The distribution of exchange rate constants was obtained for each catalyst sample from the relaxation dynamics using inverse Laplace transform deconvolution methods (30). These kinetic distributions are shown for 0.1 and 1.0 wt.% K–$Cu_{0.5}Mg_5CeO_x$ catalysts in Figs. 4b and 4c. The distribution curves were normalized to give an area of unity. The y-axis represents the distribution function $f(k)$, where

$f(k)\ dk$ gives the fraction of the total number of accessible basic sites with exchange rate constants between k and $k + dk$.

The density of sites that reversibly bind CO_2 at typical catalytic turnover time obtained by isotopic exchange methods on MgO at 573 K is 0.38×10^{-6} mol/m^2; this is lower than the value of 18.3×10^{-6} mol/m^2 reported for the surface density of oxygen atoms in MgO (31). This is not unexpected since the $^{13}CO_2/^{12}CO_2$ isotopic switch method only detects those basic sites that participate in exchange reactions near 573 K. The density of available basic sites in $Cu_{0.5}Mg_5CeO_x$ increases with increasing K loading (Table 2). Potassium also leads to slower exchange processes, suggesting that stronger basic sites form when alkali is present on modified MgO surfaces (Figs. 4b and 4c). An increase in K loading from 1.0 to 3.5 wt.% increases basic site density from 2.3 to 5.2×10^{-6} mol/m^2, but has no detectable effect on the exchange rate constant and site distribution (Table 2). The presence of small amounts of CeO_x in MgO (Mg/Ce = 5 at.) increases both the density and the strength of basic sites (Table 2).

In contrast with the CO_2 TPD method, in which both temperature and surface coverage vary with time, $^{13}CO_2/^{12}CO_2$ exchange methods probe the density and reactivity of basic sites under conditions of chemical equilibrium and constant temperature. Exchange methods also avoid contributions from the decomposition of catalytically irrelevant and unreactive carbonates and from the desorption of strongly adsorbed CO_2. This method probes the number of sites that can be made available for base-catalyzed reactions at temperatures typical of isobutanol synthesis. As we discuss below, competitive adsorption between CO_2 and aldehydic species on such sites renders basic sites unavailable for alcohol synthesis reactions on $Cu_{0.5}Mg_5CeO_x$ catalysts.

Isobutanol Synthesis from CO/H$_2$ Mixtures

Cs–Cu/ZnO/Al_2O_3 and K–$Cu_{0.5}Mg_5CeO_x$ catalysts show the highest isobutanol synthesis rates and alcohol-to-hydrocarbon product ratios among reported catalysts for the synthesis of isobutanol at low temperatures (<623 K) and pressures (6, 7, 32). Alcohol synthesis rates on K-modified $Cu_{0.5}Mg_5CeO_x$ catalysts depend strongly on potassium concentration. Intermediate K concentrations (1.0–1.5 wt.%) lead to the highest isobutanol synthesis rates and selectivities (7).

Reaction products obtained on 1.0 wt.% K–$Cu_{0.5}Mg_5CeO_x$ (583 K and 4.5 MPa) and 2.9 wt.% Cs–Cu/ZnO/Al_2O_3 (580 K and 4.5 MPa) are shown in Table 3 at similar CO conversion values. The data reported by Apesteguia *et al.* (7) on similar K–$Cu_{0.5}Mg_5CeO_x$ samples are also shown in Table 3. Methanol, isobutanol, and CO_2 were the most abundant reaction products. CO_2 is formed in CO oxidation or water–gas shift reactions, using adsorbed oxygen atoms formed directly during the synthesis of dimethylether, hydrocarbons, and higher alcohols or by the readsorption of the water formed along with these products.

TABLE 3

Activities and Selectivities for Isobutanol Synthesis on K-Promoted $Cu_{0.5}Mg_5CeO_x$

Catalyst:	Ref. (7)	This study	This study
Composition:	0.9 wt.% K $Cu_{0.5}Mg_5CeO_x$	1.0 wt.% K $Cu_{0.5}Mg_5CeO_x$	2.9 wt.% Cs Cu/ZnO/Al_2O_3
Space velocity [cm^3/g-cat.h]:	1832	1500	6000
CO conversion [%]:	15.5[a]	14.7[b]	15.4[c]
CO reaction rate [mol CO conv./g-cat.h]:	6.3×10^{-3}	4.4×10^{-3}	17.0×10^{-3}
	Carbon selectivities[d] [%]		
Methanol	57.7	62.7	67.6
Ethanol	1.9	1.7	4.4
1-Propanol	2.6	3.0	6.9
Isobutanol	10.4	6.2	6.9
Other higher alcohols and oxygenates	2.2	9.2	9.5
Dimethylether	1.2	6.8	0.9
Hydrocarbons	24.3	9.9	2.5
CO_2	31.0	23.4	22.6

[a] Reaction conditions: 593 K, 5.1 MPa, $H_2/CO = 1$.
[b] Reaction conditions: 583 K, 4.5 MPa, $H_2/CO = 1$.
[c] Reaction conditions: 580 K, 4.5 MPa, $H_2/CO = 1$.
[d] Hydrocarbon and alcohol selectivities normalized on a CO_2-free basis (except CO_2).

The higher CO_2 selectivity reported by Apesteguia *et al.* (7) may reflect the slightly higher reaction temperature in their studies and their higher selectivity to hydrocarbons. Also, higher alcohol-to-hydrocarbon ratios were obtained on our samples than on those studied by Apesteguia *et al.* (7). Our $Cu_{0.5}Mg_5CeO_x$ catalyst, however, shows much higher selectivity to dimethylether. Both hydrocarbons and dimethylether are formed on acid sites but the formation of hydrocarbons requires subsequent reactions of dimethylether. These results suggest that our samples contain fewer residual sites than catalysts of similar nominal composition reported by Apesteguia *et al.* (7), apparently as a result of more effective alkali dispersion. Potassium appears to titrate residual acid sites formed during coprecipitation or CuO reduction processes. Potassium also increases the density and strength of basic sites required for chain growth reactions of alcohols (Table 2, Fig. 4).

Alkali dispersion appears to be sensitive to the details of the impregnation procedure. For example, the addition of potassium before oxidative treatment of dry precipitates (calcination) leads to catalysts with much higher selectivity to hydrocarbons than on samples impregnated with K after oxidation. Higher potassium contents (e.g., 3.5 wt.%) are undesirable because the more complete titration of residual acid sites is accompanied by sintering of the metal oxide support and in the number of accessible Cu atoms measured

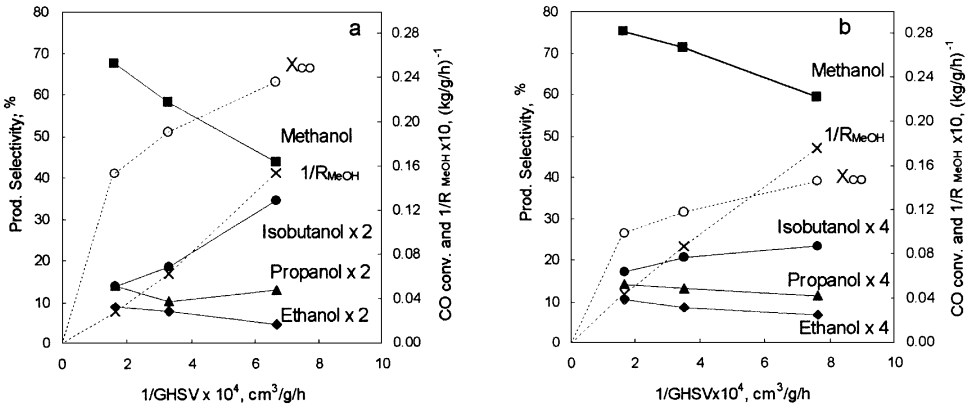

FIG. 5. CO conversion and product selectivities vs space velocity on (a) Cs–Cu/ZnO/Al_2O_3 and (b) K–$Cu_{0.5}Mg_5CeO_x$. [583 K, 4.5 MPa, $CO/H_2 = 1$. Product selectivities are on CO_2-free basis.]

by N_2O decomposition methods. These surface Cu atoms are required for methanol synthesis and alcohol conversion to aldehydes during CO hydrogenation to higher alcohols (Table 2).

The effects of space velocity (bed residence time) on alcohol synthesis rates and selectivities are shown in Fig. 5 for 2.9 wt.% Cs–Cu/ZnO/Al_2O_3 and 1.0 wt.% K–$Cu_{0.5}Mg_5CeO_x$. CO conversion should increase linearly with increasing bed residence time at the low CO conversion levels in this study. The observed decrease in the slope for the CO conversion curve with increasing bed residence time (Fig. 5) reflects the gradual approach to equilibrium by the primary methanol synthesis step and possibly also the inhibition of methanol synthesis reactions by CO_2 and H_2O formed as side products of hydrocarbon and higher alcohol synthesis. Isobutanol and higher alcohols form in secondary chain growth reactions, such as methanol carbonylation or aldol coupling reactions, which are favored by longer bed residence times. C_2–C_3 alcohols are intermediate products that undergo chain growth; therefore, their selectivity reaches a maximum value at intermediate values of residence time.

Isobutanol is a kinetic end product, because it lacks the two α-hydrogens required for facile chain growth via aldol condensation pathways. Therefore, isobutanol selectivity increases with increasing residence time. This increase, however, is less marked on K–$Cu_{0.5}Mg_5CeO_x$ than on Cs–Cu/ZnO/Al_2O_3, because base-catalyzed chain growth reactions are inhibited by CO_2 more strongly on K–$Cu_{0.5}Mg_5CeO_x$ than on Cs–Cu/ZnO/Al_2O_3. These effects are discussed in detail below. CO_2 appears to inhibit both methanol synthesis on Cu sites and aldol coupling reactions on basic sites during isobutanol synthesis reactions on K-promoted $Cu_{0.5}Mg_5CeO_x$ catalysts. The weaker basic sites on Cs–Cu/ZnO/Al_2O_3 (Table 2) appear to be less sensitive to CO_2 poisoning; as a result isobutanol selectivities reach higher values than on K–$Cu_{0.5}Mg_5CeO_x$ with increasing bed residence time.

Methanol synthesis rates decrease with decreasing space velocity on both catalysts, because the methanol synthesis reaction

$$CO + 2H_2 = CH_3OH$$

approaches equilibrium under our reaction conditions; these conditions were chosen in order to maximize yields of higher alcohols. Higher alcohol yields are obtained at higher temperatures and long bed residence times. When methanol yields become limited by equilibrium, methanol synthesis rates become proportional to space velocity, because CO conversion to methanol remains constant with increasing bed residence time.

On typical methanol synthesis catalysts (i.e., Cu/ZnO/Al_2O_3), the presence of CO_2 in modest concentrations (1–2% mol) actually increases methanol synthesis rates (33). High CO_2 concentrations (>10% mol), however, lead to higher steady-state oxygen surface coverages and inhibit methanol synthesis on these catalysts (33). Cs-modified methanol synthesis catalysts reach maximum rates at very low CO_2 concentrations (<2%) (34). Steady-state oxygen coverages during methanol synthesis on Cu surfaces depend on the relative rates of oxidation and reduction of surface Cu atoms. At high CO_2 concentrations the rate of oxidation increases relative to reduction, leading to higher steady-state oxygen coverages and to a (reversible) decrease in the number of surface Cu atoms available for methanol synthesis. These surface metal atoms on Cu crystallites catalyze methanol synthesis reactions of $CO/CO_2/H_2$ mixtures (33, 35).

In order to examine the details of CO_2 inhibition effects on methanol and isobutanol synthesis, CO_2 was systematically added to the synthesis gas feed. The results are shown in Fig. 6 as the reciprocal of methanol and isobutanol synthesis rates versus CO_2 concentrations. Typical Langmuir–Hinshelwood rate expressions would lead to straight lines when data are presented in this form. Methanol synthesis

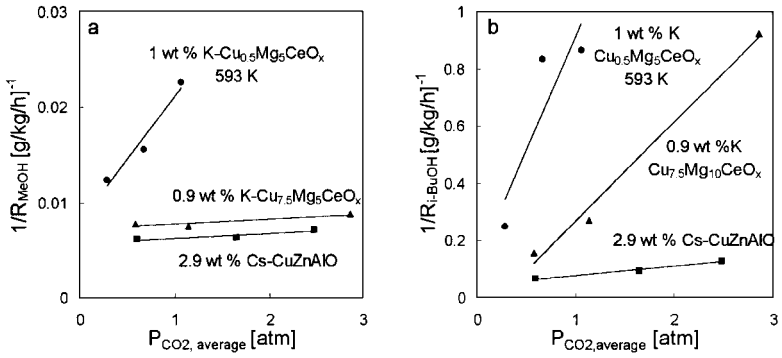

FIG. 6. Reciprocal methanol (a) and isobutanol (b) productivity vs average CO_2 partial pressure for 1 wt.% K–$Cu_{0.5}Mg_5CeO_x$, 2.9 wt.% Cs–Cu/ZnO/Al_2O_3, and 0.9 wt.% K–$Cu_{7.5}Mg_5CeO_x$. [583 K, 4.5 MPa, $H_2/CO = 1$, 3000 $cm^3/g/h$.]

rates for catalysts with high Cu contents decreased slightly as the CO_2 concentration was increased. Methanol synthesis rates on 1.0 wt.% K–$Cu_{0.5}Mg_5CeO_x$ were more strongly inhibited by CO_2. These results reflect the operation of these catalysts near methanol synthesis equilibrium. Catalysts containing a larger number of Cu surface sites (e.g., 1.0 wt.% K–$Cu_{7.5}Mg_5CeO_x$) can maintain equilibrium methanol concentrations even after a significant fraction of such sites are covered with oxygen adatoms during steady-state catalysis; therefore no effect of CO_2 on the methanol productivity is observed until larger amounts of CO_2 are added. Catalysts containing fewer Cu sites (e.g., 1.0 wt.% K–$Cu_{0.5}Mg_5CeO_x$) become unable to maintain methanol synthesis equilibrium conversions at lower CO_2 concentrations than catalysts with higher Cu site densities.

The effect of CO_2 on the rate of higher alcohol synthesis has not been as thoroughly studied as on methanol synthesis rates. Tronconi *et al.* (36) observed lower yields of higher alcohols on K–$ZnCrO_x$ at 673 K when CO_2 (3–6%) was added to the H_2/CO feed. These authors proposed that water, produced from CO_2 in the reverse water–gas–shift reaction, titrated active sites. Elliot (37) observed that higher alcohol synthesis over Cu/ZnO was enhanced by the addition of small amounts of CO_2 (6%) at 557–561 K. Calverley and Smith (38) observed that the higher alcohol yields reach a maximum at intermediate CO_2 concentrations (0–9% CO_2) on 0–0.5 wt.% K–Cu/ZnO/Cr_2O_3 at 558 K. They also observed that the effect of CO_2 becomes stronger as alkali concentration increases.

Figure 6b shows the reciprocal isobutanol synthesis rate as a function of the average CO_2 partial pressure within the catalyst bed. The catalyst with low Cu content was inhibited more strongly by the presence of CO_2 than catalysts with higher Cu contents. To some extent, this may reflect the reversible inhibition of Cu metal sites by CO_2, which leads to lower methanol yields on catalysts with low Cu content. Although methanol is not involved in the initial formation of ethanol (39) on Cu/$MgCeO_x$ catalysts, it acts as a C_1 precursor in the synthesis of 1-propanol and isobutanol from ethanol. Also, as we discuss later, aldol coupling reactions of alcohols require both Cu and basic sites; therefore any blocking of surface Cu atoms by oxygen can lead to a decrease in isobutanol synthesis rates. CO_2 inhibition of isobutanol synthesis reactions may also reflect the reversible titration of basic sites on oxide surfaces by acidic molecules, such as CO_2. The inhibiting effect of CO_2 is greater on 1 wt.% $CuMg_{7.5}CeO_x$ than on 2.9 wt.% Cs–Cu/ZnO/Al_2O_3, possibly because of the stronger basicity of the former (detected by the dynamics of CO_2 exchange). On low Cu catalysts, alcohol chain growth appear to be limited by the availability of minority Cu sites and thus CO_2 inhibition of Cu such sites decrease chain growth rates. Higher Cu contents lead to coupling rates controlled by reactions on basic sites, which are blocked by CO_2 most effectively on the more strongly basic MgO-based materials. Basic sites on 0.9 wt.% $CuMg_{7.5}CeO_x$ appears to be more sensitive to CO_2 than on 2.9 wt.% Cs–Cu/ZnO/Al_2O_3. This is consistent with the faster dynamics of CO_2 exchange on the latter catalysts.

Alcohol Coupling Reaction Pathways

Alcohol and aldehyde coupling reactions were studied in order to probe reaction pathways involved in branched and linear higher alcohols synthesis from methanol, ethanol, and propanol intermediates formed initially during CO hydrogenation reactions at high pressures. These studies also address the effects of CO_2 on alcohol dehydrogenation reactions and on chain growth reactions and the roles of Cu, K, and Mg–Ce oxides in the synthesis of branched alcohols. These experiments were carried out on Mg_5CeO_x, $Cu_{0.5}Mg_5CeO_x$, K–$Cu_{0.5}Mg_5CeO_x$, and K–$Cu_{7.5}Mg_5CeO_x$ under atmospheric pressures in a gradientless batch reactor. Two types of reactants were used: pure ethanol and $^{13}CH_3OH$–acetaldehyde mixtures.

Acetaldehyde was the initial product of reactions of pure ethanol on $Cu_{0.5}Mg_5CeO_x$ (Fig. 7). Dehydrogenation reactions occur much faster than chain growth reactions; the latter lead to the formation of acetone, *n*-butyraldehyde,

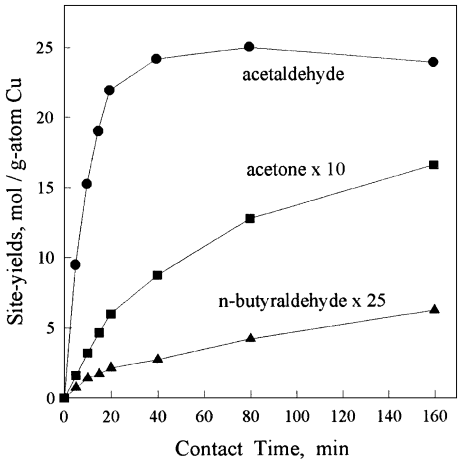

FIG. 7. Site yields as a function of contact time on 1.0 wt.% $K–Cu_{0.5}Mg_5CeO_x$ in ethanol reactions. [573 K, 101.3 kPa total pressure, 4.0 kPa ethanol, balance He.]

and other oxygenates. Site yields (*y*-axis, Fig. 7) are defined as the number of moles of ethanol converted to products per g-atom Cu (total) in the catalyst charge. The total number of Cu atoms in the sample is a convenient normalizing parameter. The local slope of the curve in Fig. 7 gives the rate of formation of each product. When divided by the fractional Cu dispersion, this becomes a site-time yield for each product, at least for reactions with rate-determining elementary steps requiring Cu surface atoms.

Acetaldehyde reaches a maximum concentration at intermediate contact times during ethanol reactions and then decreases gradually, suggesting that acetaldehyde concentrations approach equilibrium. Acetone and *n*-butyraldehyde were the predominant condensation products. The nonzero initial slopes on acetone and *n*-butyraldehyde curves are inconsistent with products formed through consecutive reactions (Fig. 7). Therefore, condensation products are either formed directly by ethanol self-condensation or via acetaldehyde condensation reactions with zero-order kinetics. Methyl ethyl ketone (by acetaldehyde self-condensation with oxygen retention reversal (40, 41)), 2-pentanone (by acetaldehyde–acetone condensation), and ethyl acetate (by ethanol–acetaldehyde reactions) were detected in much smaller concentrations among reaction products.

Reaction pathways involved in the formation of all detected products are shown in Fig. 8. Acetaldehyde is formed via ethanol dehydrogenation (step I). Aldol species (butan-1-al-3-ol) formed from direct condensation reactions of ethanol and from self-condensation of acetaldehyde produce *n*-butyraldehyde (steps II–IV) and methyl ethyl ketone (steps II–V) (40). The aldol species converts to the keto form via H transfer (step VI); methyl ethyl ketone is also formed by dehydration–dehydrogenation reactions of the keto form (step VII). Acetone is formed via two pathways: by reaction of aldol intermediates with surface oxygen followed by decarboxylation (steps VIII–IX) and by reverse aldol condensation of the keto form of reaction intermediates (step X). Formaldehyde formed in the latter reaction

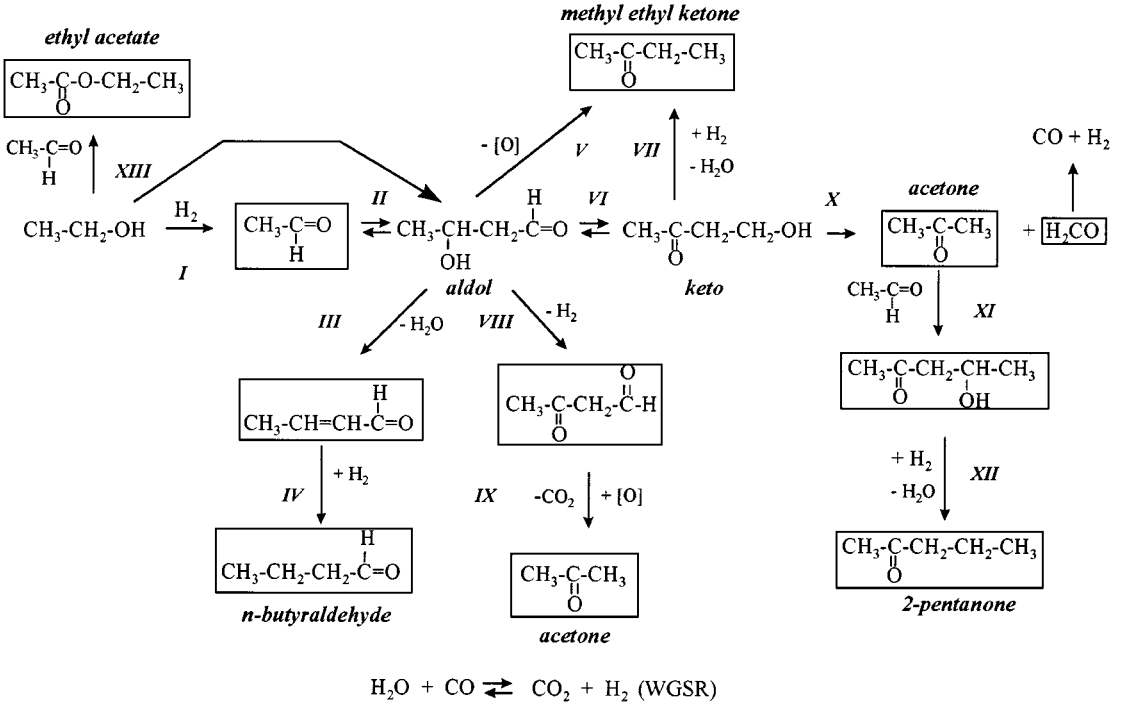

FIG. 8. Reaction scheme for ethanol reactions on $K–CuMg_5CeO_x$ catalysts.

TABLE 4

Effects of Cu- and K-Loading on Ethanol Consumption and Product Formation on Mg_5CeO_x

		Ethanol dehydrogenation		Rates of formation			
				Acetone		Butyraldehyde	
Cu (wt.%)	K (wt.%)	Areal rate r_1[a]	Turnover rate r_1[b]	Areal rate r_2[c]	Turnover rate r_2[d]	Areal rate r_3[c]	Turnover rate r_3[d]
0	0	4.0×10^{-9}	—	6.2×10^{-11}	6.5×10^{-5}	ND[e]	ND[e]
7	0.1	3.6×10^{-7}	0.24	3.0×10^{-9}	2.2×10^{-3}	4.5×10^{-10}	3.4×10^{-4}
7	1.0	2.4×10^{-7}	0.23	4.3×10^{-9}	1.8×10^{-3}	7.6×10^{-10}	3.2×10^{-4}
49	1.2	9.4×10^{-7}	0.24	4.4×10^{-8}	1.0×10^{-2}	1.2×10^{-9}	2.8×10^{-4}

[a] r_1 is the rate of ethanol consumption as mol/m^2 total · s.
[b] Turnover rates per Cu surface atom as s^{-1}.
[c] r_2 and r_3 are the rates of product formation as mol/m^2 $MgCeO_x$ · s.
[d] Turnover rates per accessible site from $^{13}CO_2/^{12}CO_2$ as mol/mol CO_2 exchangeable · s.
[e] Not detected.

decomposes rapidly to CO and H_2. 2-Pentanone is formed by condensation of aldol-type intermediates formed in acetone–acetaldehyde self-condensation reactions (steps XI–XII). Ethylacetate forms via reaction of ethanol with acetaldehyde (step XIII) (40).

Ethanol reaction rates and the selectivity to acetaldehyde, *n*-butyraldehyde, and acetone were measured on K–$CuMgCeO_x$ catalysts with a range of Cu and K concentrations in order to examine the role of individual catalyst components on dehydrogenation and condensation reaction pathways. The results are shown in Table 4. Initial reaction rates were obtained from the slopes of site-yield plots at short contact times using the total surface area, the $MgCeO_x$ surface area (estimated from the difference between the total BET surface area and the copper surface area), the number of basic sites from CO_2 exchange, or the Cu metal surface area of each sample in order to normalize reaction rates.

Initial dehydrogenation rates were very low on Mg_5CeO_x catalysts and ethanol conversion reached a limiting value of about 9% after 0.33 h; this conversion value is much lower than the equilibrium conversion predicted from thermodynamic data at these reaction conditions (90%). Ethanol conversion rates decreased markedly with increasing conversion because of (i) the formation of surface polymeric species from acetaldehyde and (ii) the inhibition effect of CO_2 (and possibly H_2O) on base-catalyzed dehydrogenation reactions on Mg_5CeO_x. Dehydrogenation rates were much higher on $Cu_{0.5}Mg_5CeO_x$, 1.0 wt.% K–$Cu_{0.5}Mg_5CeO_x$, and 1.2 wt.% K–$Cu_{7.5}Mg_5CeO_x$ catalysts than on Mg_5CeO_x, suggesting the involvement of Cu metal sites in the dehydrogenation of ethanol to acetaldehyde. The presence of K decreased areal ethanol dehydrogenation rates because of a concomitant decrease in Cu dispersion. Ethanol dehydrogenation turnover rates (normalized by exposed Cu atoms) on $Cu_{0.5}Mg_5CeO_x$, 1.0 wt.% K–$Cu_{0.5}Mg_5CeO_x$, and 1.2 wt.% K–$Cu_{7.5}Mg_5CeO_x$ catalysts were 0.24, 0.23, and 0.24 s^{-1}, respectively. Thus, ethanol dehydrogenation requires exposed Cu atoms, which become inactive for both N_2O decomposition and alcohol dehydrogenation by blockage with K species. Dehydrogenation turnover rates are not affected by Cu crystallite size or by the titration of some Cu surface atoms with KO_x species.

Aldol coupling chain growth rates are lower on Mg_5CeO_x than on $Cu_{0.5}Mg_5CeO_x$ because of the lower acetaldehyde steady-state concentrations in the former. At similar steady-state acetaldehyde concentrations on $Cu_{0.5}Mg_5CeO_x$ and 1.0 wt.% K–$Cu_{0.5}Mg_5CeO_x$ catalysts, the presence of K increases the rate of base-catalyzed aldol coupling reactions leading to acetone and butyraldehyde (Table 4). Thus, it appears that the higher basic site density and strength detected by $^{13}CO_2/^{12}CO_2$ isotopic switch measurements lead to higher rates of base-catalyzed aldol condensation reactions. The total rates of base-catalyzed aldol coupling reactions, when normalized by accessible basic sites, are similar on $Cu_{0.5}Mg_5CeO_x$ (2.5×10^{-3} mol/mol CO_2 exchangeable · s) and 1 wt.% K–$Cu_{0.5}Mg_5CeO_x$ (2.2×10^{-3} mol/mol CO_2 exchangeable · s). Aldol coupling chain growth reaction rates on 1.2 wt.% K–$Cu_{7.5}Mg_5CeO_x$ (49 wt.% Cu, 0.047 Cu dispersion) are, however, much higher than on low Cu-loading catalysts (7 wt.% Cu, 0.14 Cu dispersion), even though basic site densities are similar on these two samples. The difference in chain growth rates indicates that Cu metal sites participate in rate-determining steps required for condensation reactions. This is confirmed by the lower aldol coupling chain growth reaction rates observed on Cu-free catalysts, which is caused not only by the low concentration of required acetaldehyde intermediates, but also by the absence of Cu sites required to increase the rate of condensation steps.

The role of copper suggests a bifunctional mechanism for aldol condensation. Ethanol adsorbs dissociatively on MgO surface to form ethoxide and hydrogen species (42). Hydrogen species are then removed by migration to Cu

sites, reaction with another H species, and desorption as H_2:

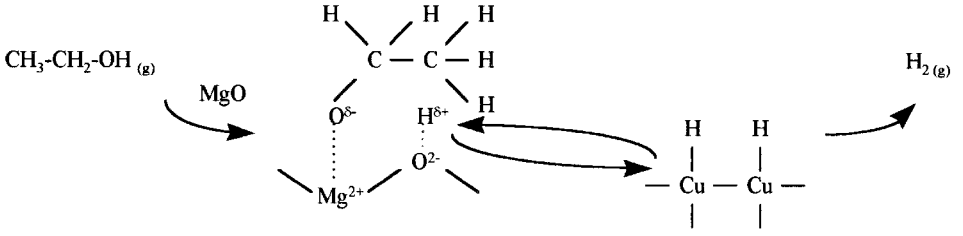

Ethoxide species then lose a β-H via intermolecular hydrogen transfer to oxygen ions and form surface acetaldehydic species:

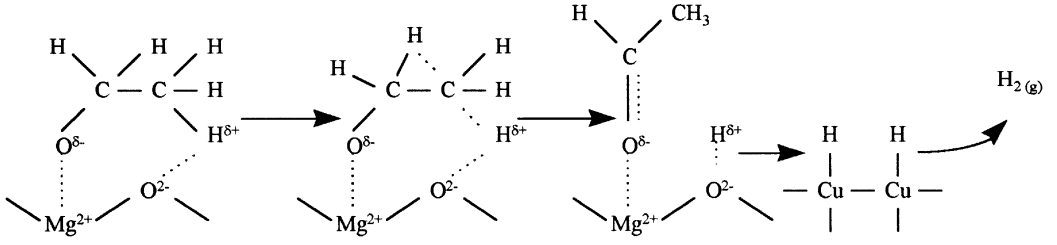

H species can migrate from basic to Cu sites and recombine on Cu sites to form H_2; as a result, basic sites become available for another hydrogen abstraction event. H–H recombination rates increase with increasing ratio of surface Cu atoms to basic sites, which is reflected by the ratio of Cu surface area to oxide surface area on K–$Cu_{7.5}Mg_5CeO_x$ (0.31) and K–$Cu_{0.5}Mg_5CeO_x$ (0.07) at similar basic site density (Table 2). The high Cu-to-oxide surface area ratio on K–$Cu_{7.5}Mg_5CeO_x$ (0.31) leads to higher aldol-condensation rates. Adsorbed acetaldehyde species can desorb as acetaldehyde, or they can undergo α-H abstraction and reaction with neighboring species to form aldol condensation products:

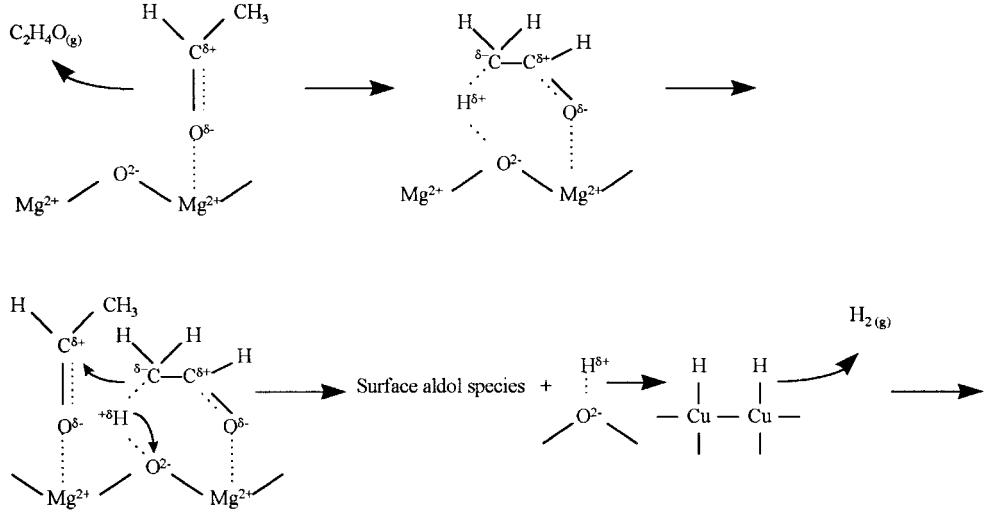

Surface aldol species can undergo reactions via the pathways shown in Fig. 8. In these reactions, the presence of copper sites enhances H transfer and provides H species for the hydrogenation of the unsaturated species (steps IV, VII, and XII, Fig. 8). It should be pointed out that the rates of the final products formed through consecutive reactions should have zero initial slopes, unless the formation of the products has zero-order kinetics. The nonzero initial slope of acetone and *n*-butyraldehyde curves (Fig. 7) is consistent with a direct pathway for the activation and conversion of ethanol in aldol condensation pathways. Additional experiments have shown that condensation, hydrogenation, and total conversion rates are approximately first order in acetaldehyde (43). Reactions of $^{12}C_2H_5OH/^{13}C_2H_4O$ mixtures

TABLE 5

Effect of CO_2 on Ethanol Reaction on K–$Cu_yMg_5CeO_x$

Product	1.0 wt.% K–$Cu_{0.5}Mg_5CeO_x$		1.2 wt.% K–$Cu_{7.5}Mg_5CeO_x$	
	Ethanol[a]	Ethanol/CO_2[b]	Ethanol[a]	Ethanol/CO_2[b]
Acetaldehyde (r_1)	2.3×10^{-7}	2.1×10^{-7}	1.2×10^{-6}	9.1×10^{-7}
Acetone (r_2)	3.9×10^{-9}	1.6×10^{-9}	7.2×10^{-8}	1.1×10^{-8}
n-Butyraldehyde (r_3)	8.0×10^{-10}	7.2×10^{-10}	1.7×10^{-9}	3.8×10^{-10}

Note. r_j are the rate of ethanol consumption and products formation as mol/m^2 total · s.

[a] $C_2H_5OH/CO_2/H_2/CH_4/He = 4.0/0/26.7/2.7/67.9$ kPa, 573 K.

[b] $C_2H_5OH/CO_2/H_2/CH_4/He = 4.0/5.3/26.7/2.7/62.6$ kPa, 573 K.

suggest that condensation reactions can proceed via direct reactions of ethanol without the intermediate formation of gas-phase acetaldehyde molecules (43).

CO_2 Effects on Alcohol Coupling Pathways

The effects of CO_2 on ethanol dehydrogenation and coupling reactions were examined on 1.0 wt.% K–$Cu_{0.5}Mg_5CeO_x$ and 1.2 wt.% K–$Cu_{7.5}Mg_5CeO_x$ catalysts by adding CO_2 (3.5 kPa, 20 kPa) to ethanol/H_2 (4.0/29.3 kPa) reactant mixtures at 573 K. Ethanol dehydrogenation rates were not affected by CO_2 addition (Table 5, Fig. 9) on both catalysts, suggesting that Cu surface atoms are not blocked by CO_2 at the conditions of our study. CO_2 also did not affect *n*-butyraldehyde formation rate on either low- or high-Cu catalysts and acetone formation rates on low-Cu catalysts. These data differ from the observed decrease in methanol and isobutanol synthesis rates as CO_2 is formed (or added) during high-pressure alcohol synthesis reactions from CO/H_2 (Fig. 6), suggesting that Cu sites are influenced by CO_2 only at the higher CO_2 pressures typical of isobutanol synthesis reactions. As discussed previously, competitive adsorption between CO_2 and acetaldehyde on basic sites may account for the observed inhibition of CO_2 on condensation reactions on 1.0 wt.% K–$Cu_{0.5}Mg_5CeO_x$ catalysts under high-pressure isobutanol synthesis conditions. The ratio of CO_2 to aldehydic intermediates is much higher during CO hydrogenation than during low-pressure ethanol reactions. Because of the lower CO_2/acetaldehyde ratio in ethanol dehydrogenation reactions, CO_2 competition for basic sites is not favorable and, therefore, the aldol coupling reactions are not influenced strongly by CO_2.The rate of acetone formation, however, decreased when CO_2 was present during ethanol reactions. CO_2 inhibition effect on acetone production may reflect: (i) the reversal of equilibrium-limited surface reaction steps that form acetone and CO_2 (steps IX and X, Fig. 8) or (ii) different parallel reaction for acetone synthesis using stronger basic sites that are more strongly inhibited by CO_2.

Cross-Coupling Reactions of $^{13}CH_3OH$–$^{12}C_2H_4O$ Mixtures

Ethanol is a useful and simple probe molecule to test the role of individual components in metal–base bifunctional catalysts for isobutanol synthesis. Ethanol reactions, however, lead to acetone and *n*-butyraldehyde, which form only 2-propanol and 1-butanol by hydrogenation during CO/H_2 reactions. 2-Propanol and 1-butanol cannot form isobutanol precursors (such as isobutyraldehyde and propionaldehyde) by condensation reactions during CO hydrogenation. ^{13}C-tracer studies of methanol-acetaldehyde cross-coupling reactions were carried out in order to examine reaction pathways leading to the formation of the C_3 and C_4 oxygenate precursors required for isobutanol formation.

Cross-coupling site yields for $^{13}CH_3OH$–$^{12}C_2H_4O$ mixtures on $Cu_{0.5}Mg_5CeO_x$ are shown in Fig. 10. The initial

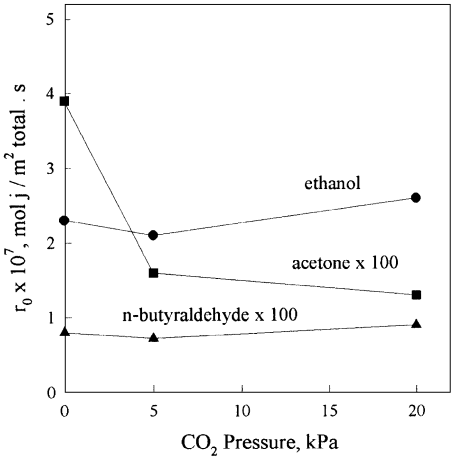

FIG. 9. CO_2 effect on ethanol reactions. Rates of ethanol consumption and of product formation as a function of CO_2 initial pressure on 1.0 wt.% K–$Cu_{0.5}Mg_5CeO_x$. [573 K, 101.3 kPa total pressure, 4.0 kPa ethanol, 26.7 kPa dihydrogen, balance He.]

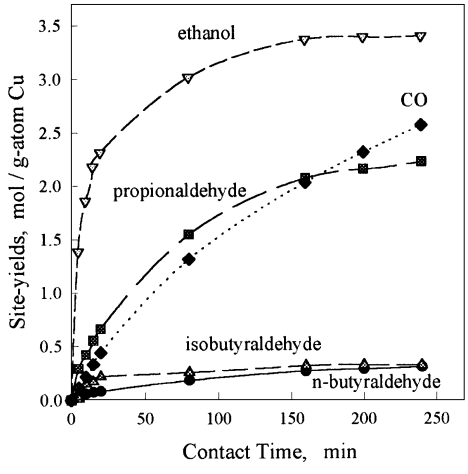

FIG. 10. Methanol–acetaldehyde reactions. Site yields as a function of contact time on $Cu_{0.5}Mg_5CeO_x$. [573 K, 101.3 kPa total pressure, 8.0 kPa methanol, 4.0 kPa acetaldehyde, balance He.]

rates (site-time yields per total mole Cu) for methanol conversion were higher than those for the conversion of acetaldehyde to ethanol and to condensation products. The $^{13}CH_3OH$ component in the feed reacted predominantly to form ^{13}CO and H_2; this reaction reverses methanol synthesis because of the unfavorable methanol synthesis thermodynamics at atmospheric pressures (but not during CO hydrogenation at high pressures). The ethanol products were predominantly unlabeled (Table 6) and formed by hydrogenation of acetaldehyde using Cu sites and hydrogen produced by methanol decomposition. Propionaldehyde contains predominantly one ^{13}C atom, suggesting that it formed by condensation of acetaldehyde with reactive formyl or methoxy-type surface species or with gas-phase formaldehyde, all formed from $^{13}CH_3OH$. The analysis of the mass spectra pattern showed that the labeled carbon was present at both the CH_3 and the CHO fragments of propionaldehyde, suggesting that aldol condensation reactions occur with retention of either one of the two oxygen atoms in aldol-keto species, as proposed by Nunan *et al.* (42, 44). They used the term "oxygen retention reversal" to indicate the oxygen atom in formaldehyde remains in the final product, whereas the oxygen of the growing intermediate in the normal aldol condensation reaction remains in the final products. Both normal and oxygen retention reversal types of aldol condensation occur on $K{-}CuMg_5CeO_x$ catalysts. These types of reactions are caused by interconversion of aldol and keto species via intramolecular H-transfer:

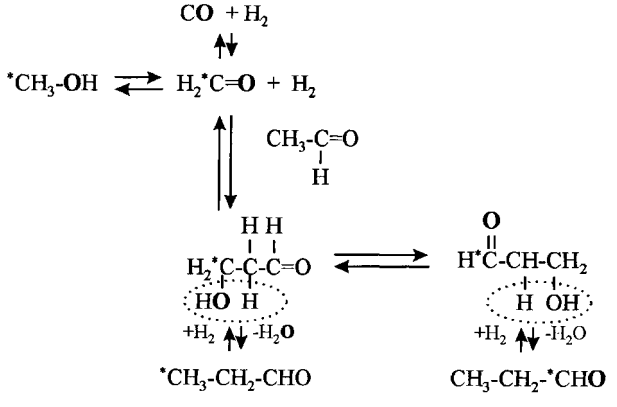

Isobutyraldehyde contained predominantly two ^{13}C atoms, suggesting that it formed by condensation of propionaldehyde (with one ^{13}C) with a C_1 species formed from methanol (Table 6). The CO_2 product of $^{13}CH_3OH{-}{}^{12}C_2H_4O$ mixtures on $Cu_{0.5}Mg_5CeO_x$ was predominantly labeled and formed from ^{13}CO via water–gas shift reactions (Table 6). Acetone and *n*-butyraldehyde showed no detectable ^{13}C-enrichment and formed exclusively via self-condensation reactions of acetaldehyde or ethanol, as observed in reactions of pure ethanol (Fig. 7). Decarboxylation of aldol intermediates to acetone explains the presence of small amounts of unlabeled CO_2. Only traces of labeled ethanol were detected among reaction products, suggesting that methanol coupling reactions, previously proposed as a route for C_1 to C_2 chain growth during higher alcohol synthesis (40), do not readily occur at the normal pressure reaction conditions of our study. In contrast with high-pressure CO hydrogenation conditions, our reaction conditions favor the decomposition of methanol and minimize its bimolecular chain-growth reactions.

TABLE 6

Carbon-13 Distribution in Products of $^{13}CH_3OH{-}C_2H_4O$ Reactions on $Cu_{0.5}Mg_5CeO_x$

	Number of carbon-13				
	0 ^{13}C	1 ^{13}C	2 ^{13}C	3 ^{13}C	4 ^{13}C
Carbon dioxide	14	86	—	—	—
Acetaldehyde	95	1	4	—	—
Ethanol	100	0	0	—	—
Propionaldehyde	0	91	6	3	—
n-Butyraldehyde	91	6	3	0	0
Isobutyraldehyde	0	0	74	23	3

Note. 573 K, 101.3 kPa total pressure, 8.0 kPa methanol, 4.0 kPa acetaldehyde, balance He.

These isotopic tracer studies are consistent with the sequence of steps shown in Fig. 11. Reverse condensation reactions of aldol and keto species (formed from $^{13}C_1$ aldehyde-type intermediate and acetaldehyde) form 1-^{13}C labeled acetaldehyde, which in turn lead to the observed propionaldehyde with 2-^{13}C atoms, isobutyraldehyde with 3-^{13}C atoms, and traces of labeled *n*-butyraldehyde. Additional studies of propionaldehyde-^{13}C-methanol coupling reactions have confirmed these isobutyraldehyde synthesis pathways. These studies have also detected the reversibility

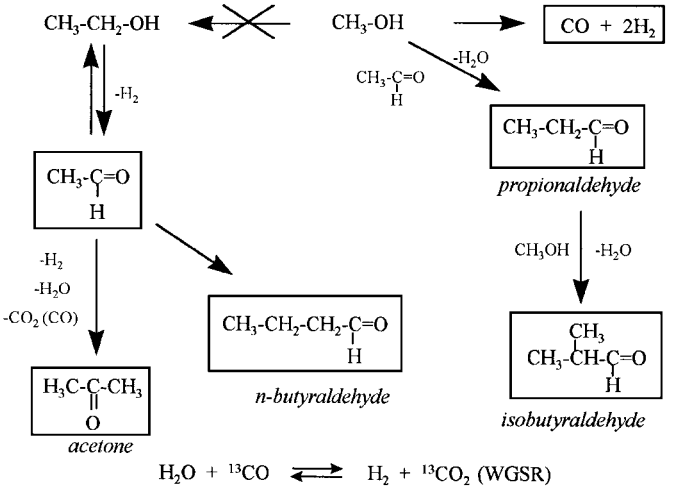

FIG. 11. Reaction scheme for methanol–acetaldehyde reactions on $K{-}CuMg_5CeO_x$ catalysts.

of aldol formation and dehydration–decarbonylation pathways. The details of these studies will be reported elsewhere (43).

Temperature-Programmed Surface Reactions of Preadsorbed Ethanol

Steady-state catalytic rates reflect the average surface properties of multifunctional and frequently nonuniform surfaces. Transient chemical reaction methods, such as TPSR, provide a useful complement to steady-state catalytic studies and isotopic switch methods. These transient methods often reveal the dynamics and "capacities" of various reactive pools available on nonuniform surfaces by varying temporally the surface coverage of preadsorbed molecules and the reactor temperature. Our initial TPSR studies have addressed the reactions of preadsorbed ethanol on $Cu_{0.5}Mg_5CeO_x$ catalysts.

The rate of product evolution during temperature-programmed surface reactions of ethanol preadsorbed on $Cu_{0.5}Mg_5CeO_x$ is shown in Fig. 12. The fraction of the adsorbed ethanol that desorbs near 350 K (Fig. 12) is likely to arise from recombination of ethoxide with H species on the surface. Ethanol appears to adsorb dissociatively on ZnO, MgO, and Cu to form surface ethoxide and hydrogen (41, 45–47). Undissociated ethanol desorbs at lower temperatures. H_2 desorbs between 373 and 523 K, leaving ethoxide species stranded on the catalyst surface. The H_2 desorption temperature decreases and the amount evolved increases when Cu is present (Fig. 12), as expected from the H–H recombination function provided by Cu and from the mobility of H-atoms on oxides near room temperature (48, 49). The broad nonsymmetric peak of H_2 suggests the presence of nonuniform desorption sites or multiple sources of H-atoms (Fig. 12b), because second-order recombinative desorption processes would lead to symmetric H_2 evolution peaks (50, 51).

Acetaldehyde is formed by additional dehydrogenation of adsorbed ethoxide species as hydrogen is depleted from the catalyst surface by Cu-assisted hydrogen desorption steps. Some acetaldehyde desorbs without further reaction, but some adsorbed aldehydic species undergo secondary reactions, such as coupling, dehydration, decarbonylation, and decarboxylation reactions to form acetone (Fig. 12). The CeO_x lattice is the likely source of oxygen atoms involved in the decarboxylation of aldol intermediates to form acetone. The reverse aldol condensation reactions (steps VI, X, Fig. 8) can also lead to the formation of acetone. The other product (formaldehyde) decomposes to CO and H_2. CO reacts with surface oxygen species to form CO_2.

CO_2 and acetone desorb at similar temperatures (about 573 K), suggesting that their evolution is limited by the kinetics of decomposition of a common intermediate leading to both products (Fig. 12). These intermediates are likely to be surface acetate species formed by nucleophilic attack of carbonyl groups within adsorbed acetaldehyde by electronegative O^{2-} species in a reducible metal oxide (e.g., CeO_2). Oxygen atoms are replenished (at least under catalytic conditions) by the water and CO_2 formed in condensation reactions. Acetate can also lead to the formation of CO, CO_2, H_2O, and H_2, as described by

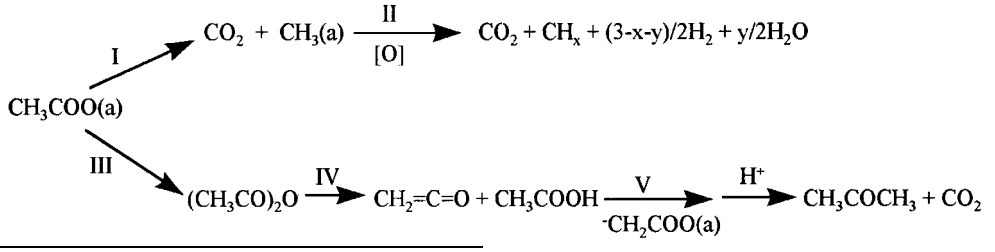

Step I: Alkyl elimination to produce CO_2 and surface alkyl species (47, 52, 53).

Step II: Alkyl decomposition to form H_2, H_2O and carbon on the surface. These surface carbon species can be oxidized by oxygen to produce carbon oxides as proposed by Barteau *et al.* on ZnO (47).

Steps III, IV: Ketene ($CH_2{=}C{=}O$), observed on ZnO (53) and on Cu(110) single crystals above 573 K (52), might form in these two steps.

Step V: $^{-}CH_2COO(a)$ surface species, formed by α-H abstraction, attacks the carbonyl group of $CH_2{=}C{=}O$, leading to the formation of acetone. A similar mechanism has been proposed for the formation of acetone from acetic acid on TiO_2 (54).

CO is one of the reactants in the conversion of synthesis gas to isobutanol. Therefore, we have also examined how CO influences the rate and selectivity in base-catalyzed aldol condensation reactions of preadsorbed alcohols. TPSR studies of preadsorbed ethanol were carried out on $K{-}Cu_{0.5}Mg_5CeO_x$ using a carrier gas consisting of 5% CO in He. As mentioned earlier, the presence of K in $Cu_{0.5}Mg_5CeO_x$ decreases the number of surface exposed Cu atoms, consistent with the lower rate of H_2 production on $K{-}Cu_{0.5}Mg_5CeO_x$ compared to that on $Cu_{0.5}Mg_5CeO_x$ (Figs. 12 and 13). Moreover, the maximum peak temperature for acetone production shifted to higher values on $K{-}Cu_{0.5}Mg_5CeO_x$. It appears that the presence of K decreases the surface concentration of acetone precursors, which in turn, causes an increase in maximum peak temperatures for second-order reactions (50).

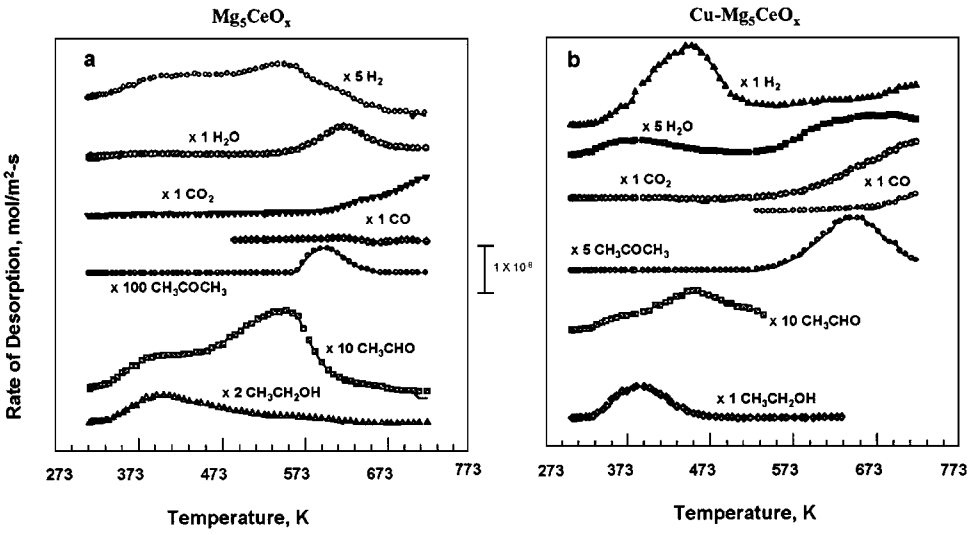

FIG. 12. Temperature-programmed surface reactions of preadsorbed ethanol on (a) Mg_5CeO_x, (b) $Cu_{0.5}Mg_5CeO_x$. [100 cm^3 (STP)/min He; heating rate, 0.5 K/s; 33.4 mg catalyst; ethanol was preadsorbed at room temperature for 10 min followed by He purging for 30 min.]

The presence of CO in the carrier gas enhanced the formation of H_2 and CO_2 via water–gas shift reactions above 523 K, markedly decreased acetone formation, and inhibited the evolution of H_2 in the low-temperature desorption peak (Fig. 13). The inhibited evolution of H_2 at low temperatures suggests that fewer Cu surface atoms are available when CO is present in He carrier gas. Cu sites may be blocked by oxygen atoms formed by reactions of CO_2 (formed from CO) with Cu surfaces on K–$Cu_{0.5}Mg_5CeO_x$. Cu clusters on Mg_5CeO_x appear to be more sensitive to oxidation (by CO_2) both during catalytic CO hydrogenation and during ethanol TPSR because of their small particle size and the possible stabilization of unreactive $Cu^{\delta+}$ species by CeO_2 (15, 16).

The presence of CO during TPSR of preadsorbed ethanol decreases the amount of acetone produced, possibly because basic sites responsible for the coupling of adsorbed acetaldehyde species are also blocked by the CO_2 formed from CO in water–gas shift or Bouduard reactions. The low concentration of surface acetaldehyde (a precursor to acetone) and the smaller number of available basic sites appear to be responsible for the marked decrease in acetone production when CO is present in the He carrier gas. More detailed TPSR results and reaction pathways of preadsorbed

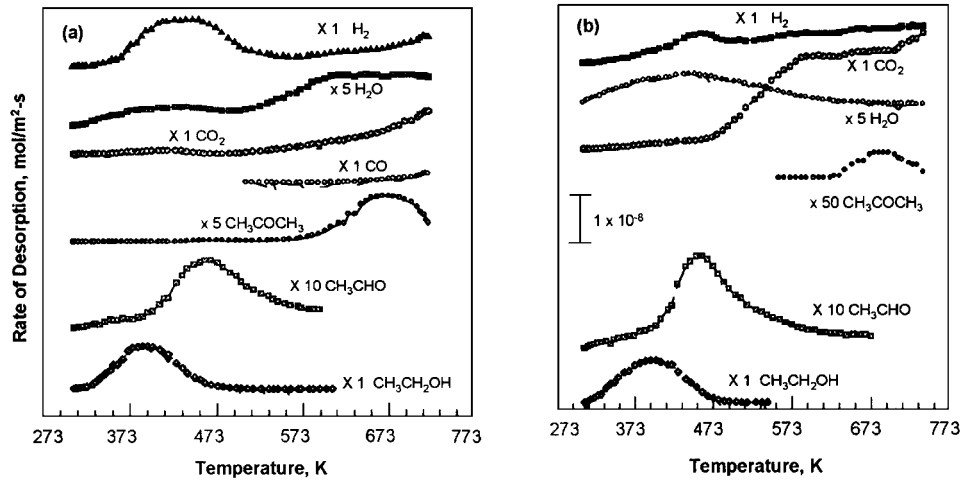

FIG. 13. Temperature-programmed surface reactions of preadsorbed ethanol on K–$Cu_{0.5}Mg_5CeO_x$ in (a) helium flow and (b) 5% CO in He flow. [100 cm^3 (STP)/min He; heating rate, 0.5 K/s; 33.4 mg catalyst; ethanol was preadsorbed at room temperature for 10 min followed by He purging for 30 min.]

alcohols and aldehydes on these samples will be reported elsewhere (15).

CONCLUSIONS

K-promoted $Cu_{0.5}Mg_5CeO_x$ catalysts are active and selective for isobutanol synthesis from CO/H_2 mixtures with high alcohol-to-hydrocarbon ratios at relatively low temperatures (583 K) and pressures (4.5 MPa). CO_2 decreases the rates of methanol and isobutanol synthesis from CO/H_2 on catalysts with low Cu concentration ($K–Cu_{0.5}Mg_5CeO_x$). Methanol production was not affected by CO_2 on catalysts with high Cu ($K–Cu_{7.5}Mg_5CeO_x$ and $Cs–Cu/ZnO/Al_2O_3$) because they operate near methanol synthesis equilibrium. CeO_2 is a structural promoter increasing both surface area and Cu dispersion. The addition of K to $CuMgCeO_x$ samples decreases Cu surface area and methanol synthesis rates, but titrates residual acid sites leading to the undesired formation of dimethylether and hydrocarbons during alcohol synthesis.

A $^{13}CO_2/^{12}CO_2$ isotopic switch method was used to probe basic site density and strength and the kinetic availability of basic sites at temperatures typical of isobutanol synthesis reactions. The addition of K increases basic site density and strength and the areal rates of aldol condensation chain growth reactions. Ethanol dehydrogenation reaction is a structure-insensitive reaction that requires Cu surface atoms. Cu sites play a critical role in condensation reaction. Alcohol chain growth reactions occur via bifunctional (metal–base) pathways requiring both Cu and basic sites. Isotopic tracer and TPSR studies of alcohol coupling reactions suggest that chain growth leading to propionaldehyde and isobutyraldehyde occurs by condensation reactions involving the addition of a C_1 species to adsorbed oxygenates.

ACKNOWLEDGMENTS

This work was supported by Division of Fossil Energy, the United States Department of Energy, under Contract DE-AC22-94PC94066. The authors thanks Mr. Zhengjie Hu for his technical assitance with isotopic switch experiments and Dr. Bernard A. Toseland (Air Products and Chemicals, Inc.) for helpful technical discussions and suggestions.

REFERENCES

1. Keim, W., and Falter, W., *Catal. Lett.* **3**, 59 (1989).
2. Keim, W., D.E. Patent 3810421 (1988).
3. Lietti, L., Forzatti, P., Tronconi, E., and Pasquon, I., *J. Catal.* **126**, 401 (1990).
4. Forzatti, P., Tronconi, E., and Pasquon, I., *Catal. Rev. Sci. Eng.* **33**, 109 (1991).
5. Sofianos, A., *Catal. Today* **15**, 119 (1990).
6. Slaa, J. C., van Ommen, J. G., and Ross, J. R. H., *Catal. Today* **15**, 129 (1992).
7. Apesteguia, C. R., Soled, S. L., and Miseo, S., U.S. Patent 5,387,570 (1995). [Assigned to Exxon Research and Engineering Co.]
8. Apesteguia, C. R., DeRites, B., Miseo, S., and Soled, S. L. *Catal. Lett.* **44**, 1 (1997).
9. Tsuji, H., Yagi, F., Hattori, H., and Kita, H., *J. Catal.* **148**, 759 (1994).
10. Radlowski, C. A., and Hagen, G. P., U.S. Patent 5,159,125. [Assigned to Amoco Corporation, Chicago]
11. Brideger, G. W., and Spencer, M. S., *in* "Catalyst Handbook," 2nd ed. (M. V. Twigg, Ed.). Wolfe Press, London, 1989.
12. Li, J.-L., and Inui, T., *Appl. Catal. A* **137**, 105 (1996).
13. Iglesia, E., and Boudart, M., *J. Catal.* **81**, 204 (1983).
14. Narita, K., Takeyawa, N., and Toyoshima, I., *React. Kinet. Catal. Lett.* **19** (1982).
15. Xu, M., and Iglesia, E. [Unpublished manuscript]
16. Lamonier, C., Bennani, A., Duysser, A., and Wrobel, G., *J. Chem. Soc. Faraday Trans.* **92**(1), 131 (1996).
17. Soria, J., *Solid State Ionics* **63–65**, 755 (1993).
18. Driscoll, D. J., Martin, W., Wang, J-X., and Lunsford, J. H., *J. Am. Chem. Soc.* **107**, 58 (1985).
19. Lunsford, J. H., Cisneros, M. D., Hinson, P. G., Tong, Y., and Zhang, H., *Faraday Discuss. Chem. Soc.* **87**, 1 (1989).
20. King, D. S., and Nix, R. M., *J. Catal.* **160**, 76 (1996).
21. Souza-Monteiro, R., Noronha, F. B., Dieguez, L. C., and Schmal, M., *Appl. Catal.* **131**, 89 (1995).
22. Garcia-Fierro, J. L., Lo Jacono, M., Inversi, M., Porta, P., Cioci, F., and Lavecchia, R., *Appl. Catal.* **137**, 327 (1996).
23. Garcia-Fierro, J. L., Lo Jacono, M., Inversi, M., Porta, P., Lavecchia, R., and Cioci, F., *J. Catal.* **148**, 709 (1994).
24. Annesini, M. C., Lavecchia, R., Marrelli, L., Lo Jacono, M., Campa, M. C., Garcia-Fierro, J. L., Moretti, G., and Porta, P., *Solid State Ionics* **63–65**, 281 (1993).
25. Campos-Martin, J. M., Garcia-Fierro, J. L., Guerrero-Ruiz, A., Herman, R. G., and Klier, K., *J. Catal.* **163**, 418 (1996).
26. Davydova, L. P., Boreskov, G. K., Popovskii, V. V., Yurieva, T. M., and Anufrienko, V. F., *React. Kinet. Catal. Lett.* **18**, 203 (1981).
27. Aleksandrov, V. Yu., Popovskii, V. V., and Bulgakov, N. N., *React. Kinet. Catal. Lett.* **8**, 65 (1978).
28. Xu, M., Hu, Z., Gines, M. J. L., and Iglesia, E. [Unpublished manuscript]
29. Boudart, M., and Djéga-Mariadassou, G., "Kinetics of Heterogeneous Catalytic Reactions." Princeton Univ. Press, Princeton, NJ, 1984.
30. DePontes, M., Yokomizo, G. H., and Bell, A. T., *J. Catal.* **104**, 147 (1987).
31. McKenzie, A. L., Fishel, C. T., and Davis, R. J., *J. Catal.* **138**, 547 (1992).
32. Nunan, J. G., Himmelfarb, P. B., Herman, R. G., Klier, K., Bodgan, C. E., and Simmons, G. W., *Inorg. Chem.* **28**, 3868 (1989).
33. Klier, K., Chatikavanij, V., Herman, R. G., and Simmons, G. W., *J. Catal.* **74**, 343 (1982).
34. Vedage, G. A., Himmelfarb, P. B., Simmons, G. W., and Klier, K., *ACS Symp. Ser.* **279**, 295 (1985).
35. Chinchen, G. C., Waugh, K. C., and Whan, D. A., *Appl. Catal.* **25**, 101 (1986).
36. Tronconi, E., Ferlazzo, N., Forzatti, P., and Pasquon, I., *Ind. Eng. Chem. Res.* **26**, 2122 (1987).
37. Elliot, D. J., *J. Catal.* **111**, 445 (1988).
38. Calverley, E. M., and Smith, K. J., *J. Catal.* **130**, 616 (1991).
39. Xu, M., and Iglesia, E., *J. Phys. Chem.* [Submitted for publication]
40. Elliot, D. J., and Pennella, F., *J. Catal.* **119**, 359 (1989).
41. Takezawa, N., Hanamaki, C., and Kobayashi, H., *J. Catal.* **38**, 101 (1975).
42. Nunan, J. G., Bogdan, C. E., Klier, K., Smith, K., Young, C., and Herman, R., *J. Catal.* **116**, 195 (1989).
43. Gines, M. J. L., and Iglesia, E. [Unpublished manuscript]

44. Nunan, J. G., Bogdan, C. E., Herman, R. G., and Klier, K., *Catal. Lett.* **2**, 49 (1989).
45. Bowker, M., and Madix, R. J., *Surf. Sci.* **116**, 549 (1982).
46. Bowker, M., Houghton, H., and Waugh, K. C., *J. Chem. Soc. Faraday Trans. 1* **78**, 2573 (1982).
47. Vohs, J. M., and Barteau, M. A., *Surf. Sci.* **21**, 590 (1989).
48. Vannice, M. A., Boudart, M., and Fripiat, J. J., *J. Catal.* **17**, 359 (1970).
49. Levy, R. B., and Boudart, M., *J. Catal.* **32**, 304 (1974).
50. Rieck, J. S., and Bell, A. T., *J. Catal.* **85**, 143 (1983).
51. Somorjai, G. A., "Chemistry in Two Dimensions: Surfaces," Cornell Univ. Press, Ithaca, NY, 1981.
52. Bowker, M., and Madix, R. J., *Appl. Surf. Sci.* **8**, 299 (1981).
53. Bowker, M., Houghton, H., and Waugh, K. C., *J. Catal.* **79**, 431 (1983).
54. Gonzalez, F., Munuera, G., and Prieto, J. A., *J. Chem. Soc. Faraday Trans. 1* **74**, 1517 (1978).